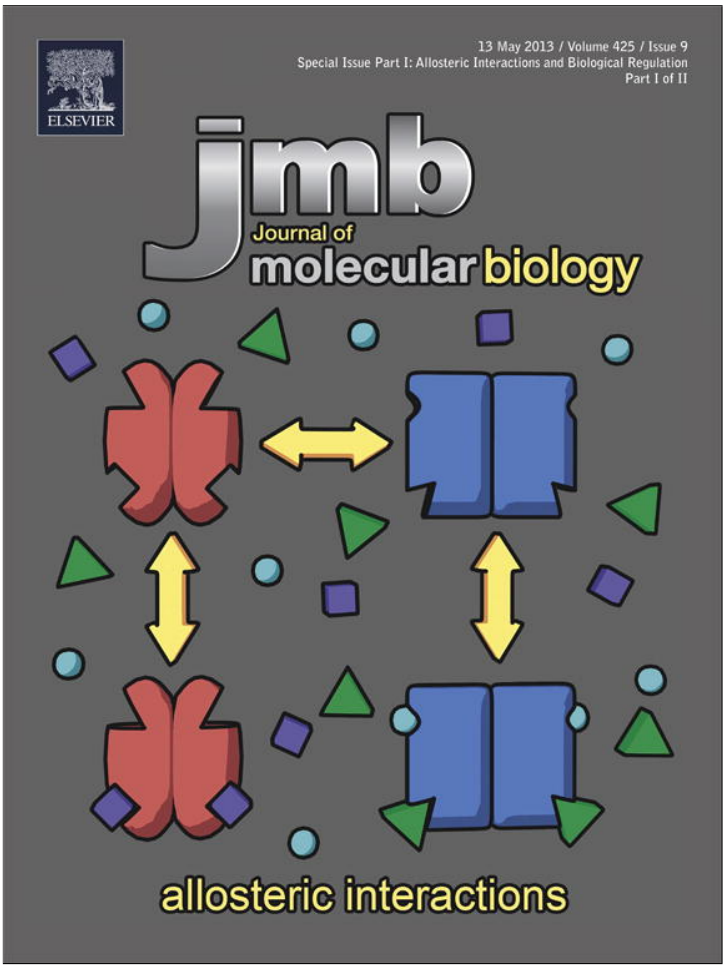

Stuart Edelstein (the editor); His overview of this special issue:

Along with applications of allosteric principles in so many diverse research areas,
progress is also continuing in the founding field of allosteric enzymes.
This subject remains very active and four communications in this issue provide examples of state-of-the-art developments
with unnatural amino acids,[49]
with chemical shift covariance analysis to follow long-range allosteric interactions,[50]
with photo-cross-linking and mass spectrometry to identify contacts between domains,[51]
and with X-ray crystallography, mutagenesis, and isothermal titration calorimetry to characterize a network of three synergistic allosteric sites.[52]

jmb Article

The Membrane-Binding Domain of an Amphitropic Enzyme Suppresses Catalysis by Contact with an Amphipathic Helix Flanking Its Active Site

Harris K-H. Huang[1], Svetla G. Taneva[1], Jaeyong Lee[1], Leslie P. Silva[2], David C. Schriemer[2] and Rosemary B. Cornell[1,3]

*1 - **Department of Molecular Biology and Biochemistry,** Simon Fraser University, Burnaby, British Columbia, Canada V5A 1S6*
*2 - **Department of Biochemistry and Molecular Biology,** University of Calgary, Calgary, Alberta, Canada T2N 4N1*
*3 - **Department of Chemistry,** Simon Fraser University, Burnaby, British Columbia, Canada V5A 1S6*

***Correspondence to Rosemary B. Cornell:** Department of Molecular Biology and Biochemistry, Simon Fraser University, Burnaby, British Columbia, Canada V5A 1S6. cornell@sfu.ca*
http://dx.doi.org/10.1016/j.jmb.2012.12.003
Edited by N. G. Ahn

Abstract

CTP:phosphocholine cytidylyltransferase (CCT), the regulatory enzyme in the synthesis of phosphatidylcholine, is activated by binding membranes using a lipid-induced amphipathic helix (domain M). Domain M functions to silence catalysis when CCT is not membrane engaged. The silencing mechanism is unknown. We used photo-cross-linking and mass spectrometry to identify contacts between domain M and other CCT domains in its soluble form. Each of four sites in domain M forged cross-links to the same set of peptides that flank the active site and overlap at helix αE at the base of the active site. These cross-links were broken in the presence of activating lipid vesicles. Mutagenesis of domain M revealed that multiple hydrophobic residues within a putative auto-inhibitory (AI) motif contribute to the contact with helix αE and silencing. Helix αE was confirmed as the docking site for domain M by deuterium exchange analysis. We compared the dynamics and fold stability of CCT domains by site-directed fluorescence anisotropy and urea denaturation. The results suggest a bipartite structure for domain M: a disordered N-terminal portion and an ordered C-terminal AI motif with an unfolding transition identical with that of helix αE. Reduction in hydrophobicity of the AI motif decreased its order and fold stability, as did deletion of the catalytic domain. These results support a model in which catalytic silencing is mediated by the docking of an amphipathic AI motif onto the amphipathic helices αE. An unstructured leash linking αE with the AI motif may facilitate both the silencing contact and its membrane-triggered disruption.

Introduction

Auto-inhibition by built-in regulatory (R) domains or separate regulatory subunits is a well-established device for many metabolic and/or signal-transducing proteins. The inhibitory interaction is relieved by ligand binding to the R subunit or by a competing interaction with another protein. Comparing crystal structures of inactive and active forms of regulatory enzymes often gives the impression of conformational switches between two rigid structures. On the other hand, evidence that highly dynamic segments are abundant in multi-domain enzymes[1] and that they can serve as regulatory switches is accumulating.[1–3] This often involves ligand or protein partner-induced ordering of a disordered segment,[2] but alternatively, some intrinsic disorder is maintained during the regulatory interaction, with only localized transient ordering.[4] For example, the disordered R domain of the CFTR (*c*ystic *f*ibrosis *t*ransmembrane conductance *r*egulator) chloride conductance channel positively modulates the channel activity by multiple transient contacts with the nucleotide-binding domain of this channel, and the contact results in only transient ordering of small segments in R.[5] In another example, a Sic1 inhibitory interaction with a single site on a cyclin-dependent kinase (Cdc4) involves multiple small

segments in Sic1 that are ordered upon contact.[6] The results on the CFTR and Sic1 systems were obtained using heteronuclear NMR experiments and comparing data in the presence and absence of the protein partners. This approach was possible because interactions were sufficiently strong between the separately expressed proteins. The regulatory interactions of many other proteins may be so weak as to require connection via the polypeptide chain and will depend on other methods to deduce them.

Our work explores the mechanism of auto-inhibition of CTP:phosphocholine cytidylyltransferase (CCT) by its regulatory M domain. CCT is a key regulatory enzyme in the biosynthesis of phosphatidylcholine (PC) and is a prototypical amphitropic enzyme. The functions of amphitropic proteins are regulated by reversible membrane binding. For CCT, membrane binding occurs in response to changes in the membrane PC content.[7,8] When the PC content declines, CCT binding to that membrane triggers its activation and this restores the PC content of the membrane.[8–10] The substrates and products of the CCT-catalyzed reaction are soluble; thus, membrane translocation does not function to promote access to these. Rather, it serves as a means to sense lipid composition. The lipid compositional sensor is a lipid-inducible amphipathic helix, domain M. Although the regulation and mechanisms of membrane binding of domain M are well understood,[11,12] regulation of catalysis by domain M is not. The same can be said for many amphitropic proteins, although progress is being made on the mechanisms of auto-inhibition for a few.[13,14]

CCT is a homodimer and each subunit consists of four regions: N, C, M, and P (see Fig. 1). A disordered N-terminal 40-amino-acid segment is followed by a 35-residue cap for the catalytic domain (region N). The 150-residue catalytic domain (domain C) is followed by the ~70-residue membrane-binding domain (domain M) and a 50-residue unstructured Ser-Pro-rich region at the C-terminus housing multiple phosphorylation sites (region P). In the soluble form of CCT, the M domain functions to suppress catalytic function[15,16] and its inhibitory conformation is unknown. Deletion of domain M increases k_{cat} ~10-fold.[17] Full activation requires membrane-triggered transformation of domain M into a 60- to 70-residue amphipathic helix[18,19] that inserts into one leaflet of the membrane, resulting in an ~100-fold elevation in k_{cat} and an ~10-fold decrease in the K_m for CTP.[17,20] Thus, domain M has dual functions as a silencer in the CCT soluble form and as an activator in the membrane-bound form. How does it do this?

Although we have determined the structure of a CCT catalytic fragment (residues 40–216) by X-ray diffraction,[21] we have not so far succeeded in generating a high-resolution diffraction pattern from crystals of a construct containing the regulatory M domain. The catalytic domain functions as a dimer with a mass of 56 kDa, making NMR analysis of a domain M footprint non-trivial. Moreover, multiple approaches to detect interactions between the CCT catalytic dimer and its regulatory tail provided *in trans* have been unsuccessful, suggesting that the interactions, if they exist, are weak and require continuity through the polypeptide chain.[17] There is other evidence supporting no more than a loose interaction between the catalytic and regulatory M domains. There was no obvious binding site for

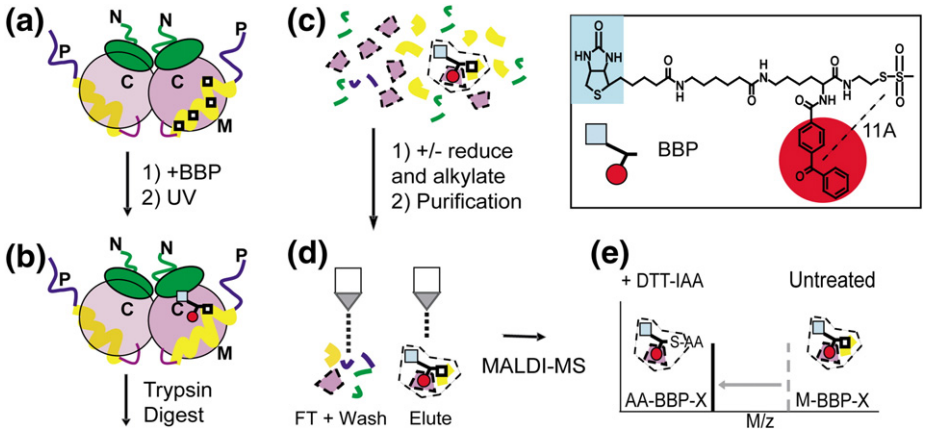

Fig. 1. Schematic of the photo-cross-linking approach to identify inter-domain contacts. (a) Single cysteines were engineered at sites within domain M (□). (b) Purified single-cysteine variants were labeled with BBP and photo-irradiated (366 nm). (c) Photo-cross-linked samples were digested with trypsin. (d and e) Biotin-tagged peptides from half of the digested sample were reduced and alkylated (DTT-IAA) prior to purification by avidin-affinity chromatography; the other half was purified without pre-treatment. Peptides were identified by MALDI-MS. The mass shift in the spectra shown in (e) is equal to the mass of the domain M peptide (with modified cysteine) minus acetamide (58 Da). Inset displays the tri-functional photo-cross-linker, BBP, which has an ~11 Å distance separation between the sulfhydryl-reactive methane thiosulfonate and the photo-reactive center of the benzophenone moiety (red) and a biotin group (blue) for peptide purification.

domain M on the catalytic domain in an analysis of the protease accessibility of CCT +/– membrane vesicles,[22] and while the catalytic domains of lipid-regulated CCTs from diverse phyla are well conserved, the M domains are not.[17] The latter finding suggests that an extensive and/or rigid structure for domain M may not be needed for silencing function. This is supported by comparative CD analysis of the secondary structure of CCT, full length and truncated, with and without lipids, which indicated that membrane binding is associated with conversion of ~60 residues in domain M from a mixture of conformers to α-helical secondary structure.[19] Domain M is also predicted to be relatively disordered by many computational algorithms,[17,23] especially its N-terminal half. The sequence of domain M and features are shown in Fig. 2a. The middle section of rat CCT is expendable, as its M domain can be replaced by the 18-residue-shorter M-sequence from *Caenorhabditis elegans* CCT, with little consequence on silencing or lipid activation.[17] The C-terminal portion is enriched in hydrophobic residues that occur in a conserved pattern, making it highly amphipathic, and has a higher predicted degree of ordering than the N-terminal region of M. Mutational analysis of CCT from *C. elegans* revealed a collaborative contribution of the C-terminal hydrophobic residues to the lipid-dependent activation and also hinted that these residues contributed collectively to the silencing function of the M domain in the absence of membranes.[24] Very recently, we showed that deletion of the C-terminal 22mer segment of domain M of rat CCT (sequence underlined in Fig. 2a) nearly eliminated silencing.[17]

As a first step to unravel the structural basis of auto-inhibition, we implemented a photo-cross-linking strategy to identify regions of contact with domain M. The approach uses full-length intact protein and places no preconceived limits on the domain M target (Fig. 1). We conjugated a tri-functional cross-linker, 2-[*N*-α-benzoylbenzoicamido-N^6-(6-biotinamidocaproyl)-L-lysinylamido]ethyl methane thiosulfonate (BBP), to sites dispersed all along domain M. BBP utilizes a methyl thiosulfonate group for disulfide exchange with engineered cysteine sulfhydryls, a benzophenone to generate a UV-induced free radical, and a flexible linker to biotin to facilitate avidin-mediated purification of cross-linked peptides following trypsin digestion (Fig. 1). This strategy using BBP has been successful in identifying sites of interaction between MutL and MutH DNA repair enzymes[25] and the α and γ subunits of cGMP phosphodiesterase.[26]

Our results revealed cross-links between several sites in domain M and the active-site region. Overlap analysis identified the most likely docking site for domain M as a pair of amphipathic helices (αE) that extend from the base of the active site. These cross-links were broken upon activation of CCT by membrane insertion of domain M or by mutagenic reduction of domain M hydrophobicity. Our data lead to a new model for CCT regulation by an auto-inhibitory (AI) motif within domain M that is delivered to the base of the active site via a flexible leash to suppress catalytic function. We suggest that regulation of CCT activity involves competition between the membrane and the helix αE dimer for the stabilization of an emergent amphipathic α-helix in domain M.

Results

Single-cysteine substitutions in domain M can form disulfide-linked CCT dimers

To carry out the BBP-mediated cross-linking study, we created single-cysteine variants in domain M, which would serve as sites for BBP conjugation. Beginning with a cysteine-free CCT[27] that has a specific activity that is approximately 50% of wild type

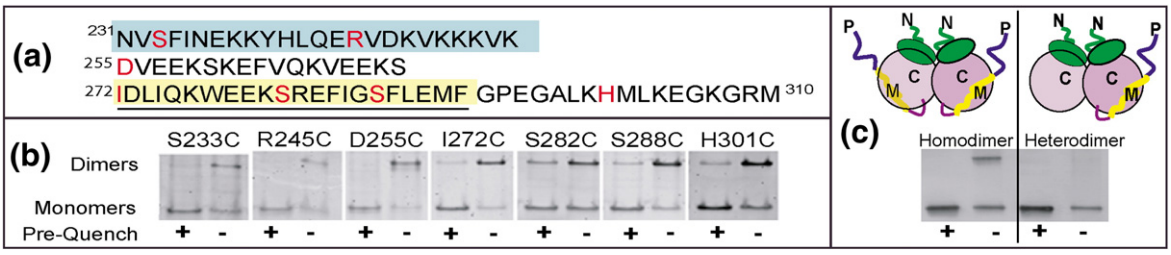

Fig. 2. Single-cysteine variants in domain M form disulfide-linked dimers. (a) Sequence of domain M of rat CCTα showing in red the sites targeted for mutagenesis to cysteine. The segment highlighted in blue is the positively charged, more disordered region of domain M. The putative AI motif is underlined and highlighted in yellow. (b) The indicated CCT variants were oxidized with copper phenanthroline. Half the samples were pre-quenched (+) with IAA. Samples were separated on nonreducing 10% *N*-[2-hydroxy-1,1-bis(hydroxymethyl)ethyl]glycine (Tricine) gels, stained with Sypro-Orange, and imaged with a Typhoon Model 9410 imager. (c) The disulfide bridge is intra-dimeric. Heterodimers composed of CCT-S288C and CCT-cat (truncated at residue 236) have only one domain M per dimer.[29] Heterodimers and homodimers of CCT-S288C (with two M domains) were oxidized with $Cu(Phe)_3$, separated by nonreducing 10% Tricine SDS-PAGE, transferred onto polyvinylidene fluoride membrane, and blotted with anti-domain M antibody.

(WT), we engineered cysteines at seven different positions along the length of domain M, targeting non-conserved sites or serines in the hydrophilic face of the M domain amphipathic helix (Fig. 2a). The specific activities of the purified single-cysteine CCTs resembled WT CCT and the cysteine-free CCT in that activity was suppressed in the absence of lipid and activated ≥20-fold in the presence of saturating lipid concentrations (Table S1). This provides confidence that the cysteine engineering was not debilitating to function or folding. A previous analysis of full-length rat CCTα dimer interface revealed inter-subunit contacts involving domain C and its N-terminal extension.[21,27] We found here that each domain-M-engineered cysteine pair can forge a disulfide bridged dimer upon oxidation (Fig. 2b). To discern whether the disulfide bridges formed because of random collisions between dimers, we prepared a heterodimer with a single M domain[28,29] (Fig. 2c). This species did not undergo disulfide formation upon oxidation (Fig. 2c), indicating that the disulfide bridges were generated between subunits of a dimer. There are two possible explanations for the domain-M-mediated intra-dimer disulfide bridges. Either each of the analogous residues in the M domains are close to each other in a stable complex or there is sufficient flexibility along the length of domain M to allow brief inter-chain contact that could be trapped by disulfide bonding.

BBP labeling was cysteine directed, and photo-activated cross-linking was efficient

The BBP cross-linking data we set out to collect would only be meaningful if shown to be restricted to cross-links between the engineered cysteine and a benzophenone-mediated target linkage. The experiments in Fig. 3, using CCT-H301C as a representative, verify that BBP conjugation was efficient and was targeted specifically to the engineered cysteine, that excess unconjugated BBP was removed prior to photolysis, and that the benzophenone-mediated photolytic cross-linking was efficient. Conjugation with BBP greatly reduced the amount of CCT disulfide-linked dimer (Fig. 3a, upper gel; compare lanes 1 and 2), consistent with efficient BBP coupling to the cysteine SH. BBP conjugation, monitored with Streptavidin horseradish peroxidase (HRP), was blocked by alkylation of cysteine with iodoacetamide (IAA; Fig. 3b), indicating strict specificity for cysteine. Excessive washes with dimethyl sulfoxide (DMSO) and then buffer succeeded in removing all unconjugated BBP from the sample (Fig. 3c). Prior to UV irradiation, the BBP adduct was sensitive to reductant (β-mercaptoethanol), but after irradiation, it was resistant to β-mercaptoethanol (Fig. 3a, lower gel; compare lanes 5 and 6), showing that it had forged a covalent cross-link to another site on the protein via the benzophenone.

The CCT tertiary fold before and after the BBP-labeling procedure appeared to remain unaltered in that its proteolysis pattern was identical (Fig. S1). The activity of the CCT variants was tested after the labeling and photo-cross-linking procedure in the presence of reducing agent to cleave any cross-links. The treated CCTs remained active and lipid dependent (Fig. S1). These results indicate that the photo-labeling procedure was not destructive of folding or function. Thus, cross-linking results would reflect interactions of the native enzyme.

Photo-cross-linked species were identified by comparative analysis of samples before and after reduction/alkylation

To identify cross-linked species, we digested the labeled CCTs to completion with trypsin and isolated

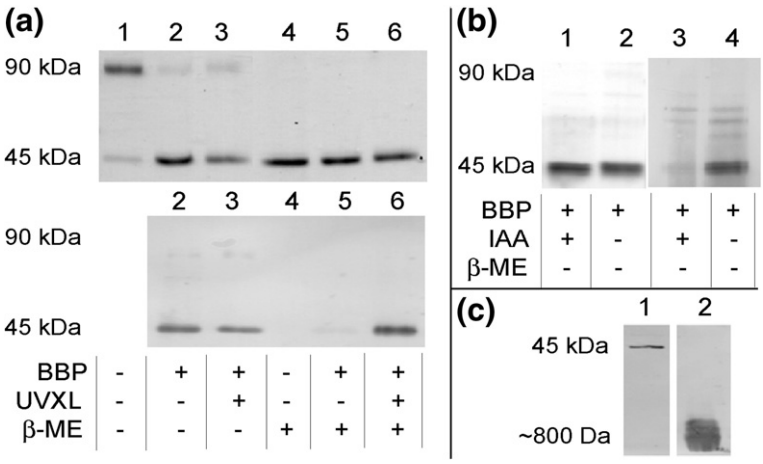

Fig. 3. Efficiency and selectivity of BBP conjugation and photo-cross-linking. (a) Conjugation and photo-labeling efficiency exemplified using CCT-H301C. Top panel: Sypro-Orange stained 10% Tricine SDS-PAGE of unlabeled (lanes 1 and 4), BBP-labeled (lanes 2 and 5), and photo-labeled (lanes 3 and 6) CCT-H301C. Bottom panel: The same samples as shown in the top gel were processed for detection of biotin-containing BBP with Streptavidin HRP. (b) BBP labeling is disulfide dependent. Silver-stained SDS-PAGE (lanes 1 and 2) and Streptavidin HRP blot (lanes 3 and 4) for samples pre-quenched with IAA prior to addition of BBP *versus* unquenched BBP-labeled CCT-H301C. (c) Washing protocol removes excess free BBP. Streptavidin HRP blot of BBP-labeled CCT-H301C after labeling, washing six times, and elution from Ni-agarose (lane 1). An equivalent amount of unconjugated BBP input is shown in lane 2. Samples were run on 16.5% Tricine SDS-PAGE.

biotinylated species by monomeric avidin-affinity chromatography. To facilitate the identification of photo-cross-linked sites, we reduced and alkylated half of the trypsin-digested samples prior to affinity purification by avidin beads (Fig. 1). This treatment cleaves the photo-cross-linked peptides at the site of cysteine conjugation, transfers the BBP to the new target site, and generates an alkylation-dependent mass shift for peptides that contain a benzophenone-mediated BBP adduct. Thus, there were four analysis conditions for each CCT variant (Fig. 4). We used the following criteria to certify a peak in the mass spectrum as a *bona fide* BBP-generated cross-linked peptide: (1) it was unique to the spectrum for the photo-cross-linked sample; (2) its mass after reduction/alkylation was reduced by an amount equivalent to the mass of the released domain M peptide, less 58 Da due to acetamide alkylation of the freed sulfhydryl of the BBP; and (3) it matched a CCT peptide theoretical mass within 1 Da.

The certification process is illustrated in the set of spectra from an analysis of CCT-H301C, shown in Fig. 4. The peak in Fig. 4c at 3116.8 Da, unique to the photo-labeled sample, matches the mass of a species that links two domain M peptides via BBP ($M_{[301–304]}$-BBP-$M_{[284–300]}$). After reduction of the disulfide and alkylation, this species generates two peptides: residues 284–300 conjugated to acetamide-modified BBP (AA-BBP-$M_{[284–300]}$), which corresponds to the 2683.2-Da peak shown in Fig. 4d, and acetamidated 301–304, which disappears from the spectrum since it no longer carries BBP and was removed during avidin-affinity purification. Also illustrated in this figure are two species at 3050 and 2353 Da unique to the photo-labeled, unreduced samples (Fig. 4c) representing cross-links between $M_{[301–304]}$ and domain C peptides, $C_{[79–94]}$ or $C_{[187–196]}$. Upon reduction and alkylation, these species produce the BBP-conjugated and acetamidated domain C peptides at 2616 and 1918 Da, respectively, shown in the bottom panel.

Sites throughout domain M forge cross-links with a region flanking the active site

CCT variants with single cysteines at position 245, 272, 288, or 301, spanning most of domain M, were analyzed under the four conditions shown in Fig. 4. The percent of total matrix-assisted laser desorption/ionization (MALDI) peaks unique to the photo-cross-linked spectra that were assigned to CCT tryptic peptides was >80%. To facilitate a comparison of the cross-linking patterns from different BBP sites, we generated photo-cross-linked peptide coverage

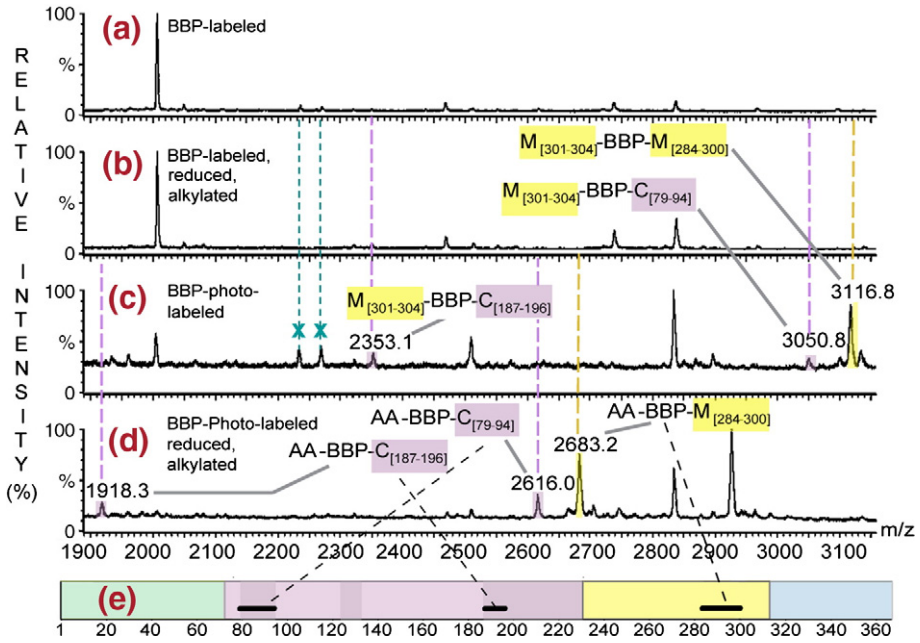

Fig. 4. Illustration of the method for assigning *bona fide* cross-links. One half of BBP-labeled CCT-H301C was UV irradiated (c and d), and the other half was not (a and b). After both samples were digested with trypsin, one portion was reduced with 100 mM DTT and alkylated with IAA (b and d); the other portion was not reduced (a and c). Samples were purified with monomeric avidin beads and analyzed by MALDI-MS. Violet and gold broken lines indicate peaks that were specific to photo-irradiated samples and that shifted mass upon reduction and alkylation, revealing the species cross-linked to the domain MC301 site. Cyan broken lines show examples of peaks that were not unique to the photo-labeled sample spectra. These were not selected for identification. (e) assigns some of the BBP-containing cross-linked peptides to the domain map of CCT. Regions N, C, M, and P are colored green, pink, yellow, and blue, respectively.

maps, as illustrated in Fig. 4e, which maps several of the peaks from the CCT-H301C spectra to the position they occupy in the CCT sequence. Supplemental Material provides representative spectra of photo-cross-linked peptides from the four domain M single-cysteine variants that were used to build these maps (Fig. S2) as well as a complete list of photo-cross-links unambiguously identified for each CCT (Table S2).

Figure 5a–d compares the peptide coverage maps of the four single-cysteine variants. A striking observation is that all four share similar photo-cross-linking patterns. All variants show relatively unfocussed photo-cross-links to domain P and within domain M, as well as cross-links to the N-terminus of domain N. The cross-links to N and P likely reflect the intrinsic disorder in these domains,[17,21–23] which would enable them to sweep out a large arc to collide with the BBP conjugated to the domain M site. In general, the most intense peaks from the irradiated samples matched to domain M peptides. These included photo-cross-links to peptides proximal to the site of conjugation, as well as self-cross-links, that is, a benzophenone-mediated cross-link to a site

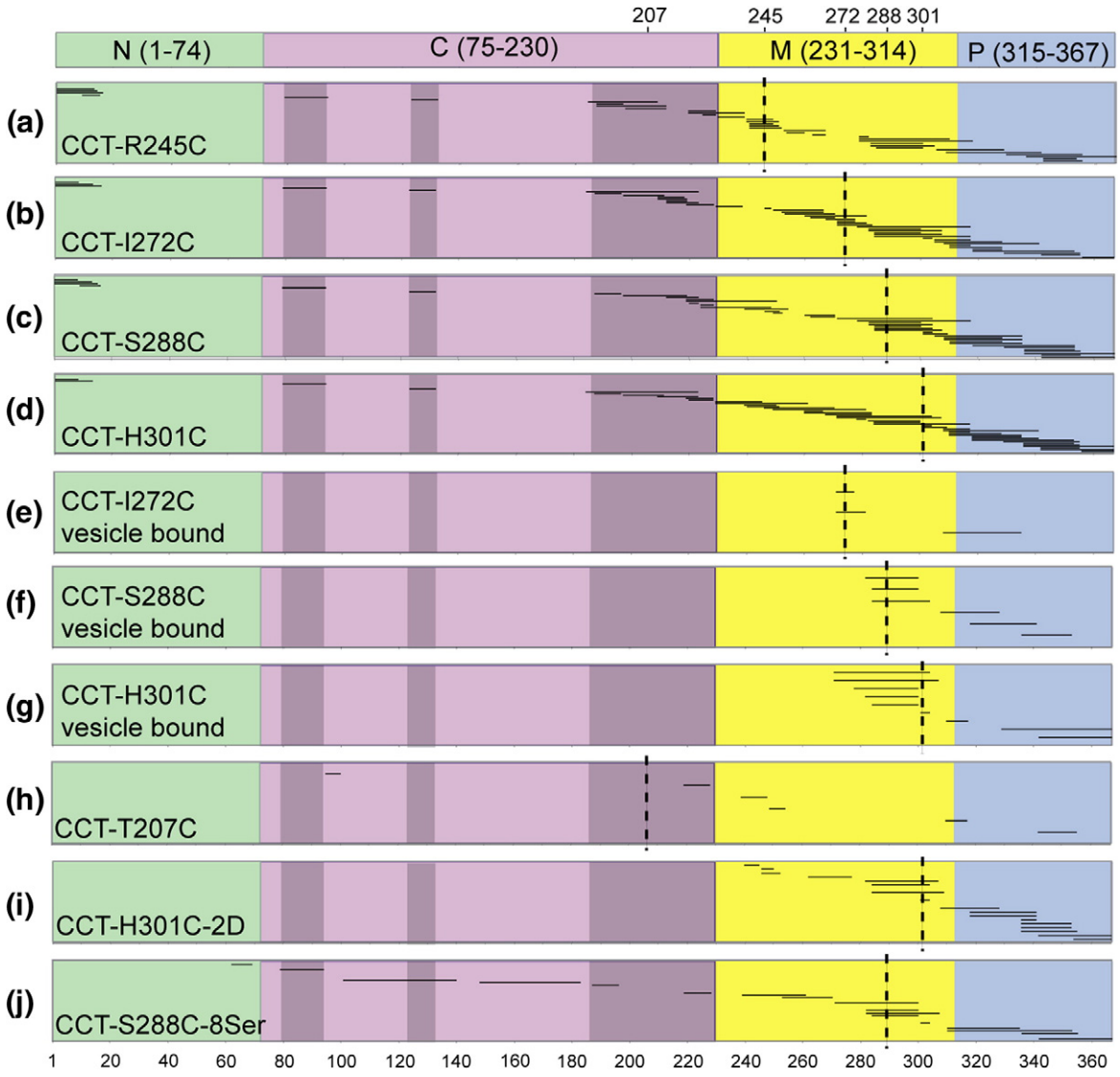

Fig. 5. Photo-cross-linked peptide coverage maps for CCT variants. The broken vertical lines indicate the position of the BBP-modified cysteine in each variant. Each horizontal line represents a peptide photo-cross-linked to the BBP-modified cysteine, identified via MALDI-MS using the stringent criteria described. Only peptides with masses that match a single theoretical peptide mass are shown. Some peptides contained missed cleavage sites. The three darkened areas in domain C mark the location of photo-cross-links common to all four variants in the soluble form. To generate membrane-bound CCTs in (e)–(g), we incubated CCTs with ~4000 molar excess DOPG sonicated vesicles prior to photolysis. Each map is a composite of at least two trials.

within the same tryptic peptide housing the cysteine site of conjugation. The high probability of cross-links within domain M is expected since this is a nearest neighbor analysis.

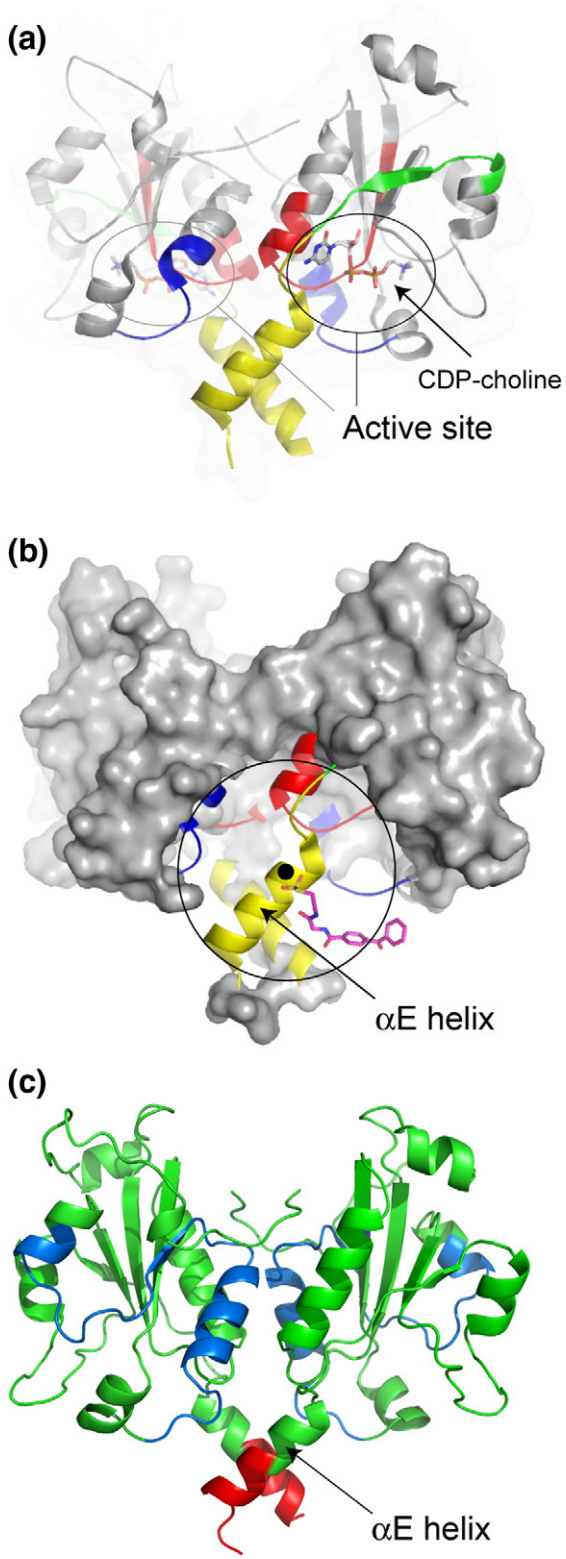

Of greater interest were photo-cross-links to domain C. These cross-links were limited to specific regions and excluded large segments of the catalytic domain (see blank regions in the coverage maps, Fig. 5). The absence of cross-links was due to neither failure of trypsin cleavage in these regions nor failure to detect such peptides in the MALDI-mass spectrometry (MS) analysis. Peptides from these regions, such as $C_{[101–122]}$, $C_{[148–162]}$, and $C_{[163–183]}$, were detected in the digest of CCT-H301C prior to purification on avidin beads (Table S3). Thus, their absence after avidin purification likely reflects lack of a biotin adduct; that is, they were not BBP cross-linked. Similar results were obtained for CCT-S288C, CCT-I272C, and CCT-R245C.

We mapped the BBP-cross-linked peptides from domain C onto the solved structure of CCT-cat,[21] Protein Data Bank (PDB) ID: 3HL4, a CCT variant truncated at residue 236 at the end of the catalytic domain. These peptides form part of the active site. They map close to the dimer interface proximal to where CTP binds,[21] to the L2 loop that contains Lys122 (which is thought to facilitate the transition state at the α-phosphate),[21,30,31] and to helix αE and the linker extending from αE to domain M (Fig. 6a). We identified residues 201–205 on helix αE as the converging contact region; that is, the site within 11 Å of all common photo-cross-linked domain C peptides (Fig. 6b and Fig. S3). Helix αE could serve as a site for domain M to dock onto and exert auto-inhibition. To further probe helix αE as a docking site for domain M segments, we engineered a single

Fig. 6. Mapping domain M–domain C contacts. (a) Common domain C peptides map to the active site. Cartoon representation of the catalytic domain of CCT (PDB ID: 3HL4) with four common cross-linked peptides highlighted on both chains of the dimer: residues 79–94 (red), 123–132 (blue), 187–196 (green), and 197–216 (yellow). (b) Convergence point of the cross-linked peptides. The convergence point (residues 201–205 on helix αE) was determined by overlap analysis of all atoms within 11 Å of the four common cross-linked peptides (for details, see Fig. S3 and Methods in Supplementary Information). When a BBP molecule (shown as pink sticks, without the biotin and linker) is centered at that site via its sulfhydryl-reactive group, the benzophenone can access each of the cross-linked peptides. The benzophenone access zone is shown as a hollowed-out sphere of 11 Å radius, and atoms within this zone are shown in colored cartoon representation. Atoms outside this sphere are in surface representation (gray). (c) H/D exchange difference map of CCT-cat *versus* CCT-312. CCT-cat contains domains N and C. CCT-312 contains N, C, and M. Green color indicates no significant difference. Red indicates a reduction and blue indicates an increase in deuteration in CCT-312 *versus* CCT-cat. The change in the helix αE peptide was from 65% deuterated in CCT-312 to 85% deuterated in CCT-cat; the statistical probability of identical deuteration for this peptide in both CCTs was $P<0.01$. More details are provided in Table S4.

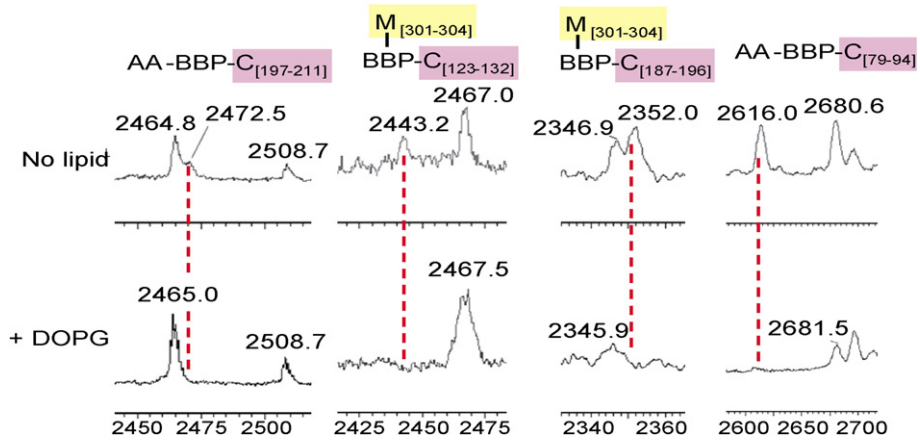

Fig. 7. Domain C cross-linked peptides are absent from spectra of CCT bound to lipid vesicles. BBP-labeled CCT-H301C was photo-cross-linked at 4 °C in the absence of DOPG (top spectra) or in the presence of 4000 molar excess DOPG (bottom spectra) and digested with trypsin. BBP-containing peptides were purified with monomeric avidin beads and analyzed on MALDI-MS as described in Materials and Methods.

cysteine at site 207 in the middle of helix αE. Photo-cross-linking analysis revealed only a few cross-links (Fig. 5h), but these did include three distinct peptides that map to domain M. The weak cross-linking outcome with BBP at Cys207 may reflect constrained orientations within a stable helical structure, BBP orientation interference by the docked M domain segment, or the interference of domain M docking by the bulky BBP at residue 207.

Hydrogen/deuterium exchange MS confirms helix αE as the domain M docking site

To validate the results obtained from the photo-cross-linking approach, we subjected two CCT constructs to hydrogen/deuterium (H/D) exchange MS analysis. CCT-cat encompasses residues 1–236, domains N and C only. CCT-312 is a truncation at residue 312 and includes domains N, C, and M. We anticipated that a domain M docking site within domain C would show a reduced deuteration level in the construct containing the M domain. Both CCTs were simultaneously exposed to D_2O for 120 s, quenched, and digested, and the peptides were separated and identified by mass. The peptide deuteration levels mapped onto the coordinates for CCT-cat (PDB ID: 3HL4) concurred with the accessibility and foldedness apparent from the solved structure, with lowest deuteration levels (<20%) for the β-sheet scaffold and dimer interface and higher deuteration levels at the periphery and connecting loops. Of the 57 peptides obtained for CCT-cat and 68 peptides for CCT-312, only 2 peptides showed significantly lower deuteration levels in CCT-312 *versus* CCT-cat. Of the two, residues 208–217 showed the largest mass shift. This peptide maps to helix αE (see red helix in the difference map, Fig. 6c). The other peptide is located in the disordered N-terminus and showed a smaller mass shift compared to the change in the αE peptide (Table S4). Six peptides showed small but significant increases in deuteration in CCT-312, represented in blue in Fig. 6c. These changes could reflect increased dynamics or accessibility for these segments in CCT-312. The H/D exchange analysis on CCT-312 also showed high levels of deuteration for domain M, confirming the open, flexible structure for this domain that we obtained in the photo-cross-linking analyses.

Lipid binding eliminates cross-links with domain C and orders domain M

If the cross-links between domain M and the catalytic domain reflect *bona fide* inter-domain contacts and function in silencing CCT activity in its soluble form, then they should be broken upon membrane binding. Indeed, peptides mapping to domain C were absent from the mass spectra of CCT-H301C photo-irradiated in the presence of ~4000 molar excess of activating lipid in the form of small vesicles (Fig. 7). The similar intensities of peaks flanking the domain C peaks in the spectra plus or minus lipid verify that the change is specific to the domain C sites. We failed to find peptide-lipid conjugates in the spectra, but lipidated peptides are notoriously difficult to detect by MALDI-time of flight (TOF)-MS, and the delipidation protocol prior to MS analysis could have extracted and removed the lipidated peptides. The analyses of vesicle-bound CCTs (Fig. 5e–g) indicate that membrane binding prevents BBP-mediated cross-bridging between C272, C288, or C301 in domain M and the domain C active site as well as the N-terminus. Photo-cross-links to region P were reduced in number and variety, and cross-links within domain M were no

longer unfocussed but restricted to sites of immediate proximity. This likely reflects a transition from a relatively unstructured domain M to an ordered, α-helical state. These results are consistent with the hypothesis that these contacts are auto-inhibitory but do not constitute proof.

Substitution of hydrophobic to polar residues in domain M and the effects on domain C contact and silencing

Although CCT M domains from evolutionarily divergent species are not well conserved, a C-terminal 22-residue portion contains a conserved pattern of hydrophobic residues, including a conserved FLEMF motif between residues corresponding to 289–293 of rat CCTα[17] (Fig. 8a). Mutation in the *C. elegans* CCT of the first phenylalanine in the FLEMF motif to an aspartate resulted in an ~12-fold increase in lipid-independent activity,[24] and in rat CCTα, loss of the entire 22mer (residues 272–293) results in an increase in lipid-independent activity that is nearly equivalent to excision of the entire regulatory region (~10-fold).[17] We hypothesized that non-conservative mutations in this AI motif would result in the disruption of contacts with the catalytic domain and subsequent loss of auto-inhibition. We mutated the two phenylalanines in the FLEMF motif to aspartates in rat CCT-H301C to produce CCT-H301C-*2D* and analyzed the effects on photo-cross-linking via BBP conjugated to position 301. This CCT variant did not generate any photo-cross-links to domain C (Figs. 5g and 8b), consistent with a disruption of contacts between the C-terminal end of domain M and domain C. However, the auto-regulation remained similar to the parent, CCT-H301C, with a mere 2-fold enhancement of the lipid-independent activity and similar activation by PC/phosphatidylglycerol (PG) (1/1) vesicles (Fig. 8d). This somewhat surprising result suggests that the contact at or near residue 301 with the catalytic domain is not required for inhibition of catalysis. Other sites must contribute to the silencing and, perhaps in so doing, compensate for the loss of contact from this site as a result of mutation at FLEMF.

To target more potential sites mediating silencing, we generated a mutant in which 8 hydrophobic residues in this 22-residue motif were changed to serine in the context of a single cysteine at position 288, CCT-S288C-*8Ser*. In the *C. elegans* CCT simultaneous switching of 4 hydrophobic residues in the 22mer segment to serine resulted in ~8-fold increase in lipid-independent activity.[24] Similarly, the rat CCT-*8Ser* mutant showed an ~7-fold increase in lipid-independent activity relative to the parental variant (Fig. 8d). In this figure, the lipid-independent activities are expressed as a fraction of the activities obtained in the presence of saturating lipid vesicles and are compared to that of CCT-cat, which is missing the entire regulatory tail. CCT-cat has compromised activity (V_{max} = ~3500 units/mg) compared to fully activated WT CCT (V_{max} = ~13,000 units/mg). This is because domain M in its lipid-bound α-helical state has a positive effect on catalysis that cannot be achieved in CCTs lacking domain M.[17] The fractional activity value for the *8Ser* variant was ~15% or approximately one-half of the constitutive activity associated with loosing the entire regulatory tail.

The photo-cross-linking pattern of the rat CCT-*8Ser* variant (Fig. 5j) differed from its parent in that cross-links were unfocussed over most of the protein between the domain N/C junction and the C-terminal tail. This could be attributed to increased disorder in domain M (see denaturation data to follow) giving rise to a broader spectrum of contacts with domain C, whereas the more hydrophobic WT version of the AI segment would spend more time in the vicinity of helix αE. However, there was one notable segment that was not captured by the cross-linker in the CCT-*8Ser* variant—the segment including helix αE at the end of the catalytic domain to the start of domain M (Figs. 5j and 8c). This segment was a prominent site for cross-linking with all single-cysteine variants in domain M. Our interpretation is that loss of hydrophobicity in the AI motif resulted in a gain in activity, increased entropy and home range for this segment of domain M, and reduced contact with αE and the domain C/M linker. Thus, effective silencing may require domain M contacts with helix αE and the linker segment.

Anisotropy values for sites in domain M are intermediate between those of domain C and the extreme C-terminus

When domain M engages the membrane, there is evidence that the entire region between residues 234 and 302 forms an ordered amphipathic helix.[18,19] The unfocussed cross-links for domain M in the soluble form of CCT (Fig. 5) suggested a high degree of conformational dynamics.

We probed domain dynamics further by fluorescence anisotropy. Our goal was to compare domain M dynamics to that of domain C, which is a tight fold with expected high anisotropy,[21] and the C-terminal tail, which is unfolded and more isotropic.[22] We conjugated Oregon Green (OG) to each of five CCT variants with single-cysteine sites in domain M, to a CCT variant with a single cysteine at position 359 at the end of domain P, and to the construct composed of residues 1–236 (CCT-cat). CCT-cat contains four cysteines in folded regions of the catalytic domain plus one other cysteine in the disordered N region. OG is an environmentally insensitive fluorophore with a 4.1-ns lifetime. In support of this, steady-state fluorescence intensities (which are related to the lifetime) for OG adducts at the different sites were very similar (Table S5). Thus, differences in

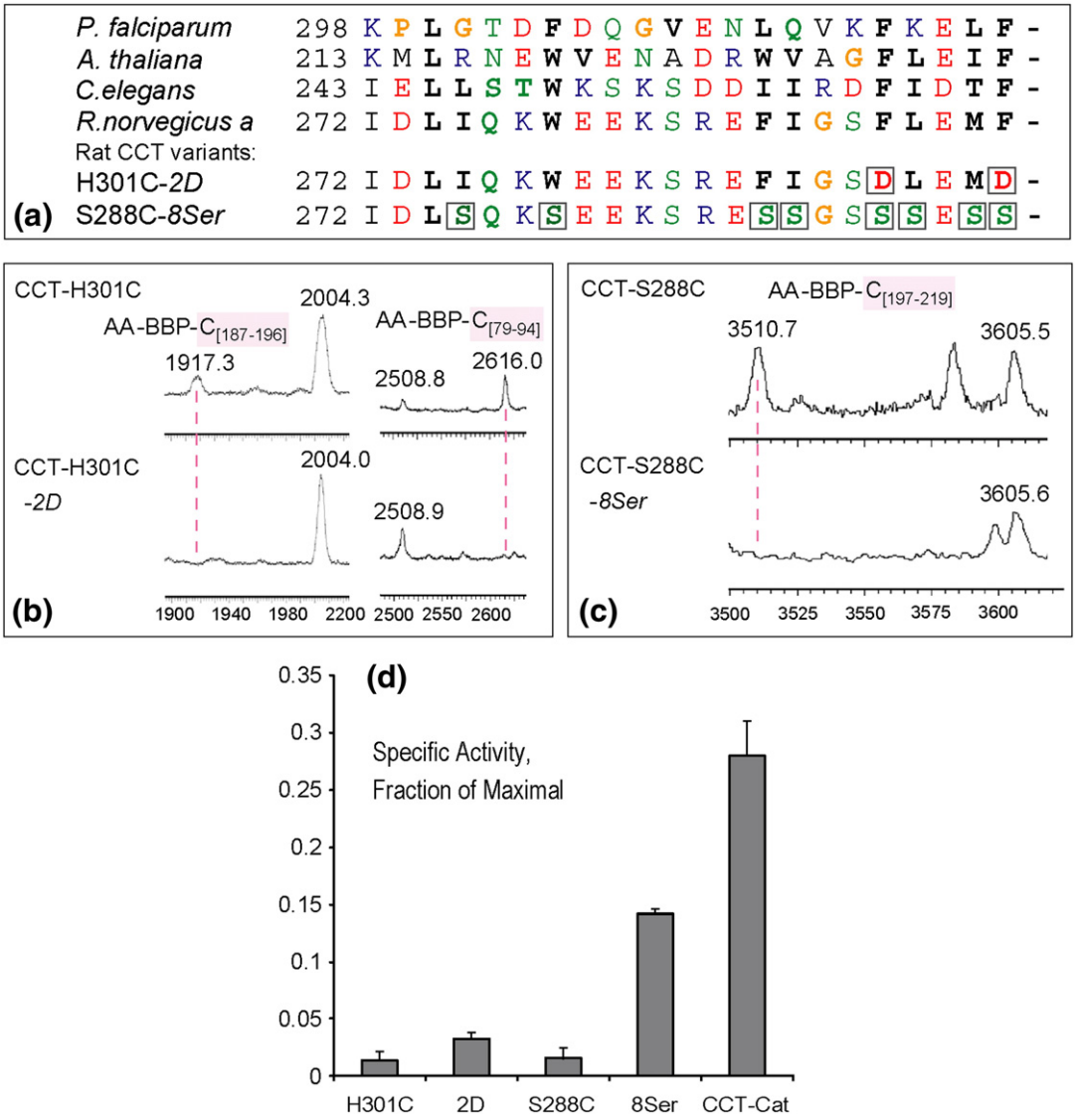

Fig. 8. Mutations that reduce hydrophobicity in the AI motif eliminate contact with helix αE and weaken silencing function. (a) Alignment of 22mer AI segment required for silencing. The mutated residues in the *2D* and *8Ser* variants are shown in gray boxes. (b and c) Examples of MS peaks corresponding to photo-cross-linked domain C peptides that are absent in CCT-H301C-*2D* (b) or CCT-S288C-*8Ser* (c). Spectra in (b) and (c) are from BBP-photo-labeled, reduced, and alkylated samples. (d) Activity of the indicated variants is expressed as a fraction of its specific activity obtained in the presence of saturating PC/PG (1/1) vesicles. For CCT-cat, the activity is expressed as a fraction of the activity of full-length WT CCT in the fully active state. Data are means ± standard error of the mean of three independent determinations.

fluorescence anisotropies reflected differences in rotational freedom at each position, instead of changes in local polarity. Similar to BBP-labeled CCT, OG-labeled CCT remained auto-inhibited in the absence of lipids and was fully activated in their presence (Fig. S4).

Since CCT is a homodimer and since OG has a small Stokes shift, we considered the consequences of homo-FRET (*f*luorescence *r*esonance *e*nergy *t*ransfer) between OG-labeled subunits. FRET reduces the anisotropy of emitted light as it increases the angular displacement of the emission oscillator.[32] Indeed, the anisotropy of OG decreased with the percent doubly labeled CCT dimers (Fig. S5). Therefore, we measured anisotropy over a range of labeling conditions and extrapolated to zero percent double-labeled dimers to obtain the FRET-free anisotropy value for each CCT mutant (Table 1). From these values, we calculated estimates for the rotational correlation times (Table 1). CCT-cat had the highest anisotropy (0.267 ± 0.011), and CCT-359C had the lowest (0.115 ± 0.004). The anisotropy values

Table 1. Domain dynamics: anisotropy of sites within three regions of CCT

Domain	Construct	Position of OG	Anisotropy	θ (ns)
C	CCT-cat	37, 68, 72, 113, 139	0.267±0.011	9.6±1.3
P	CCT-359C	359	0.115±0.004	1.8±0.1
M	CCT-S233C	233	0.222±0.007	5.7±0.4
M	CCT-R245C	245	0.208±0.010	4.9±0.5
M	CCT-I272C	272	0.215±0.006	5.3±0.3
M	CCT-S288C	288	0.206±0.006	4. 8±0.3
M	CCT-H301C	301	0.225±0.007	5.9±0.4
M	CCT-H301C-*2D*	301	0.183±0.005	3.8±0.2

FRET-free steady-state anisotropy values were obtained by extrapolation from the plot shown in Fig. S5. Rotational correlation times (θ) were calculated using the following formula: $r = r_o/(1+\tau/\theta)$, where r is the anisotropy, the fluorescence lifetime is $\tau = 4.1$ ns, and the limiting anisotropy is $r_o = 0.381$.

of OG at sites in domain M were similar to each other and fell intermediate between the ordered and disordered extremes. The rapid correlation times, ranging from 2 to 10 ns, reflect variation in segmental protein motion. The correlation time for tumbling of the whole CCT dimer (90 kDa) would be in the vicinity of 50–60 ns.[32]

We anticipated that anisotropy would increase at each domain M site upon binding of CCT to lipid vesicles. Indeed, this was the case when the fluorophore was positioned at residue 245 in the polar and positively charged portion of domain M, where the anisotropy increased from 0.179 to 0.230 (Table 2). However, the anisotropy either stayed the same or decreased slightly upon membrane binding at the sites associated with the C-terminal AI motif. This somewhat surprising result suggested that, while the N-terminal portion of domain M has less structure in the soluble form *versus* the membrane-bound form, the AI motif in the CCT soluble form is ordered to the same extent as a membrane-bound, amphipathic helix.

Table 2. Effect of lipid vesicles on anisotropy of sites within domain M

Section of domain M	Position of OG	Trial	Lipid: CCT	Anisotropy
Leash	245	I	0	0.181±0.002
Leash	245	II	0	0.176±0.003
Leash	245	III	0	0.177±0.001
Leash	245	I	400	0.228±0.001
Leash	245	II	400	0.230±0.002
Leash	245	III	900	0.221±0.001
Leash	245	II	1200	0.236±0.002
AI	272	III	0	0.213±0.001
AI	272	III	800	0.192±0.001
AI	288	III	0	0.205±0.003
AI	288	III	750	0.202±0.003
AI proximal	301	III	0	0.214±0.001
AI proximal	301	III	750	0.198±0.001

Single-cysteine variants were labeled with OG, and the percentage of total labeling was determined. Steady-state anisotropy values were obtained in the presence or absence of the indicated molar excess of a sonicated suspension of egg PG/L-α-lyso-PC (1/4). This micellar lipid mixture eliminates light scattering and fully activates CCT (19). Results from three separate preparations of labeled CCT-R245C and single preparations of labeled CCT-I272C and CCT-H301C are shown. The percent of dually labeled CCT dimers ranged from 1% to 20% in these trials.

Unfolding transitions for the AI motif and helix αE are similar

To compare the fold stability of the different portions of CCT, we examined urea-induced unfolding transitions, monitoring OG anisotropy at the various sites. OG-labeled CCT-cat was relatively resistant to urea, requiring 4.0±0.1 M urea for the unfolding transition (Fig. 9a and Table S6). The unfolding transition was weakly cooperative, likely due to the heterogeneity of the five cysteine sites. As a second check for this unfolding transition, we monitored the fluorescence anisotropy of a single intrinsic tryptophan located at residue 151, buried at the base of the active site.[21] It showed an unfolding transition very similar to that of the OG (3.8±0.1 M urea) but was more cooperative (Fig. 9a and Table S6). By comparison, the site on the flexible C-terminus (CCT-C359) had low anisotropy in the absence of urea, which declined progressively and without resistance between 0 and 2 M urea. OG-labeled domain M at residue 233 at the extreme N-terminus of domain M and sites 272, 288, and 301 within or flanking the C-terminal AI motif showed denaturation responses that were intermediate between CCT-cat and CCT-C359 (Fig. 9b and Table S6). Clear unfolding transitions were observed near 2 M urea, significantly lower than that of CCT-cat. We then asked, how does the unfolding transition of these domain M segments compare with that of the putative domain M docking site on helix αE? The results were quite striking: the unfolding behavior of the domain M sites was nearly identical with that of helix αE, tagged with OG at residue 207 (Fig. 9b, red curve). Both undergo unfolding midpoints at 2 M urea. This result is suggestive of a domain M–αE connection at some level.

The unfolding transition monitored at residue 245 differed from the other domain M sites, with a transition midpoint appearing at <1 M urea, indicative of more disorder at this portion of domain M compared to the other sites probed. The sequence surrounding residue 245 is much more polar than the other domain M sites we probed.

To test the hypothesis that contact with helix αE induces order within or flanking the AI region of domain M, we examined the urea-induced unfolding behavior of the M domain in isolation from the catalytic domain using a construct composed of domains M+P only (CCT tail). The anisotropy at

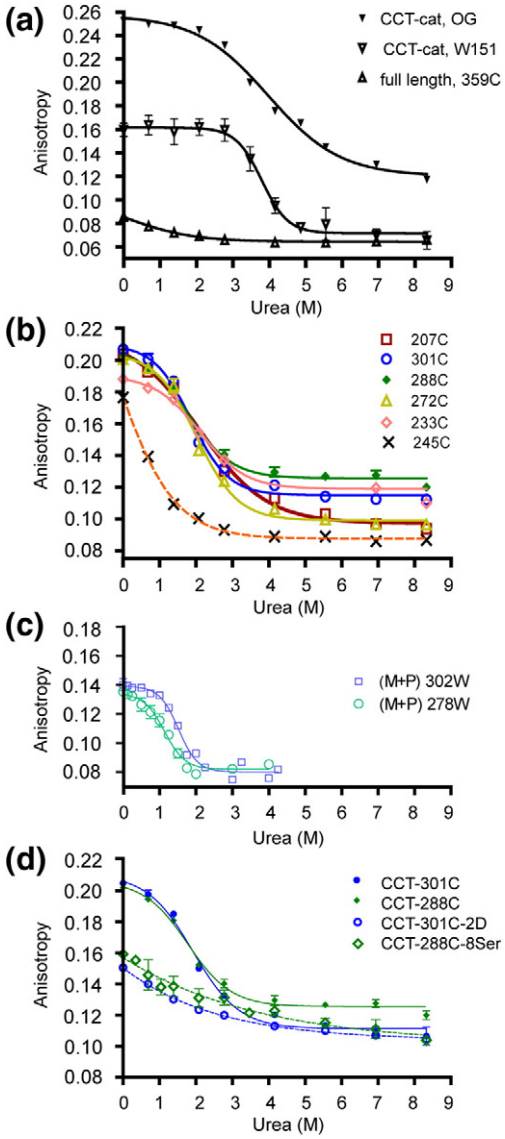

Fig. 9. Domain M sites show unfolding behavior that resembles that of helix αE. OG-labeled CCT samples were treated with the indicated concentrations of urea for 5 min and their steady-state anisotropies were analyzed at 20 °C, with six acquisitions for each sample. Data are means ± standard error of the mean of two independent determinations.

sites 278 and 302 retained some resistance to urea, but the unfolding midpoint was shifted to 1.1 and 1.5 M, respectively (Fig. 9c and Table S6). By comparison, the unfolding midpoint monitored at sites 272 and 301 occurred at 2.0 ± 0.1 M urea in full-length CCT, which provides helix αE as a putative docking site (Fig. 9c and Table S6). These data suggest that domain M possesses weak intrinsic structure at its C-terminal portion that is strengthened by interactions with helix αE.

Reduced hydrophobicity in domain M variants correlates with decreased order

Loss of domain M cross-links to the αE helices of the catalytic domain accompanied the substitution of two (CCT-H301C-*2D*) or eight (CCT-S288C-*8Ser*) nonpolar residues to polar residues near the C-terminus of domain M (Fig. 5i and j). These substitutions also greatly reduced the anisotropy and folding stability of the region adjacent to the substitutions (Table 1 and Fig. 9d). The mutations are likely to elevate the degree of disorder thereby reducing contact time with helix αE. For the *2D* mutant, the disordering and disruption of contact with αE must be highly localized since silencing was only slightly reduced, whereas for the *8Ser* mutant, the disordering is likely spread over the entire 22-residue AI motif.

Discussion

Domain M interacts with αE helices of the CCT catalytic dimer

At the onset of this project, the physical mechanism whereby the catalytic activity of CCT is regulated by the reversible membrane binding of its lipid-inducible amphipathic helix (domain M) was completely unknown. The approaches used in this work, while low resolution, have unveiled an inhibitory inter-domain contact in the enzyme's soluble, silenced form without any previous clue as to where that might be.

We identified cross-links between multiple sites within domain M and the portion of the active site proximal to the dimer interface. Overlap analysis of the cross-linked peptides converged on helix αE at the base of the active site. If a segment of domain M carrying the BBP cross-linker docks onto this helix, the benzophenone could easily access the three common domain C cross-linked peptides, the αE helix itself, and peptides in the linker region between domains M and C. When the cross-linker was conjugated to a site in helix αE, reciprocal contacts were captured to domain M peptides. That helix αE is a key site of interaction with domain M was confirmed by deuterium exchange analysis. Helix αE is an amphipathic helix that contributes to the interface of the catalytic dimer by interacting with αE′ in the other subunit, and it makes contact with the CTP substrate and with both products.[21,30,33]

What portion of domain M makes contact with helix αE? The BBP cross-linking analysis suggested that multiple segments over the whole length of domain M make the contact. However, our probing of domain dynamics/fold stability shed more light on this question. We observed nearly identical anisotropy

values and unfolding transitions for αE and domain M sites 272, 288, and 301, located within or flanking the C-terminal AI motif. The unfolding transitions were intermediate between the rigid tertiary fold of the catalytic core and the very disordered C-terminus of the protein. In the solved structure of CCT-cat (3HL4), the two αE helices segregate from the rest of the protein at the base of the catalytic domain fold and interact with each other via nonpolar side-chain van der Waals contacts involving Ile206, Ile209, Val210, and Tyr213 and with the catalytic domain via a set of just three hydrogen bonds between helix αC and Arg208 in αE.[21] Thus, the unfolding of domain M at these sites resembled the unfolding of a dimeric amphipathic α-helix with little additional tertiary structure. We refer to this folded state as molten globular to reflect high secondary but low tertiary structure. Molten globular structure was eliminated by mutations that reduced domain M hydrophobicity. Our urea denaturation analysis provided evidence that the C-terminal portion of domain M has preformed structure but that the presence of the catalytic domain with its αE helices as a docking platform served to reinforce this intrinsic structure. Preformed secondary structure at the C-terminal section of domain M is in accord with poor proteolytic accessibility of this portion in the soluble form of full-length CCT[22] and predictions of disorder probability.[17,23] It has been argued that small pre-folded islands in a structurally plastic domain can offer an advantage to the energetics of protein–protein interactions.[34]

When the fluorophore was positioned at residue 245 at the N-terminus of domain M, the unfolding transition was characteristic of an intrinsically disordered segment. Moreover, there was a significant increase in anisotropy at this site upon addition of lipid vesicles, suggestive of an unfolded to folded transition. There is evidence from work with CCT from *C. elegans* that this portion of domain M, which is deficient in hydrophobic character, has minimal influence on silencing, since a truncation in the middle of domain M that retained this region was constitutively active.[35] Residue 245 may reside in a flexible hinge (or leash) that serves to bring the C-terminal, more hydrophobic region of domain M to dock onto amphipathic helix αE. CD data,[19] disorder predictions,[17,23] and the inter-subunit disulfide bridging and unfocussed intra-domain M BBP cross-linking data we presented here for rat CCT argue against a stable α-helical structure for the entire M domain in the soluble form but are compatible with a small, pre-folded α-helical segment (e.g., the primary AI motif) on a flexible leash. With BBP attached to Cys245, we also failed to capture a cross-link with a helix αE peptide (209–218), which was prominently cross-linked to the other domain M sites. Preferred docking of the AI motif may have precluded docking of domain M segments in the flexible region near Cys245. However, docking of the AI motif might bring the BBP at Cys245 into close enough contact with the catalytic domain to allow cross-links with domain C peptides.

The leash portion of domain M is likely to facilitate the transition between the docked, inhibitory AI motif, and the membrane-induced amphipathic helix spanning both the leash and the AI motif. The N-terminal section of M is strongly positively charged in all CCTs. Thus, when the membrane negative-charge density increases, electrostatic attraction with the leash portion would act as a physical force to dissociate the AI motif from αE. The leash folds into an amphipathic helix on the membrane surface and pulls the helically poised AI segment into place for one continuous ~70-residue amphipathic helix. In support of the importance of leash electrostatics, progressive elimination of positive charge in the leash led to progressively lower membrane affinity.[36,37]

Do the properties of helix αE make it a good candidate for a domain M docking site? In the crystal structure of the CCT catalytic domain (PDB ID: 3HL4), chain B contains an ordered helix αE extending from Thr202 to Val215. In chain A, helix αE is visible to Tyr216 but is distorted at Tyr213. The ends of the visible portions of the two αE helices make contact with two αE helices of another CCT dimer in an adjacent layer of the crystal lattice.[21] In other words, helix αE pairs form a surface favorable for interaction with other helices. Helical structure is strongly predicted by several algorithms to extend to residue 222 followed by a strongly predicted turn at ^{223}RGY and, as such, would create a 22-residue amphipathic helix, with a hydrophobic moment of 0.41.[38] The lack of observable electron density for residues 217–236 and the high thermal factors for residues 210–216 in 3HL4 imply structural flexibility. We suggest that all these elements of helix αE make it ideal for the docking of short amphipathic segments from domain M, which may stabilize their helical structure as well as that of helix αE, in a process of synergistic folding. Figure S6 displays the surface of the CCT catalytic dimer from the vantage point of domain M. The helix αE pair is manually extended to residue 221, creating an exposed and fairly continuous hydrophobic surface over a length of ~20 residues. This surface could easily accommodate the docking of ≤20-residue amphipathic helices from the C-terminal portion of domain M. The cross-linking results from analysis of two mutant versions of CCT suggested a role for hydrophobic contacts between domain M and helix αE, which is consistent with an amphipathic structure for both segments. Tail regions of invertebrate CCTs containing the 22mer AI motif but with variation in some hydrophobic amino acids can substitute for the rat CCT tail in chimeric enzymes with respect to lipid-

dependent regulation of activity.[17] Thus, the helix αE–AI interaction may be adaptable (slippery) rather than a rigid lock-and-key. Future work will systematically examine reciprocal roles of hydrophobic residues in both domain M and helix αE in the docking and silencing mechanisms.

Docking of the AI segment of domain M onto helix αE silences CCT

What is the evidence that the contacts between domain M and helix αE contribute to inhibition of catalysis? First, the contacts were not captured in the membrane-bound active form of CCT. They were associated only with the soluble, auto-inhibited state. Second, no contacts with helix αE were captured by cross-linking in the partially deregulated domain M mutant (CCT288C-*8Ser*) with eight substitutions at hydrophobic residues in the putative AI motif. Moreover, this mutant lacked an unfolding transition resembling that of helix αE. The serine substitutions increased disorder in this region of domain M. The dispersed contacts with the catalytic domain may reflect defective targeting to helix αE and a fully disordered and longer leash for the BBP at site 288 in this CCT variant. Because CCT-*8Ser* domain M spends less time docked on helix αE, it is a less-effective silencer. However, when two phenylalanines within the most conserved element of the AI segment[17] were changed to aspartates, contact in the immediate vicinity with αE was broken, but the silencing function was preserved. Thus, multiple compensating contacts within the AI motif may mediate silencing.

This model is reminiscent of the mode of inactivation of tetrameric potassium channels by amphipathic segments tethered to a flexible leash.[39–41] Each subunit contains an inactivating segment, but only one is required for plugging the channel, suggesting an alternating mechanism of interaction with the channel pore. Similarly, the CCT dimer requires only one domain M for effective silencing.[29] Docking on the pair of αE helices can explain this finding since either M domain segment would have equal access to them.

How could interaction of the domain M AI motif with helix αE inhibit catalytic function? In the solved structure of the rat CCT catalytic dimer (PDB ID: 3HL4) and of the bacterial analog, GCT (PDB ID: 1N1D), a side chain (Thr202 in CCT) at the N-terminus of helix αE interacts through an ordered water with the α-phosphate of the product, CDP-choline.[21,30] Moreover, in a solved structure of GCT-CTP (PDB ID: 1COZ),[33] backbone NH groups at the residues corresponding to Thr202 and Ser203 in rat CCT make direct contact with the β- and γ-phosphates of CTP. Thus, helix αE likely participates in multiple steps during the catalytic cycle. Binding of domain M segments may interfere with one or more of those steps via deformation of αE. Additionally, there is evidence for cooperativity of the two active sites of the dimer.[29] Binding of the AI segments may disrupt dimer contacts at the helix αE crossover to weaken the cooperative interactions of the two active sites. Lastly, docking of the AI segments at the base of the active sites may impede access of substrate to the active site, accounting for the low CTP K_m for the CCT soluble form.[17,20] The identification of the sites in CCT mediating the negative regulation of catalysis has established a crucial base for elucidating the mechanism of auto-inhibition.

Materials and Methods

Construction, expression, and purification of variants of rat CCTα

Single cysteines at codons 233, 245, 255, 272, 282, 288, 301, and 359 were introduced using QuikChange mutagenesis into a cysteine-less full-length CCT in pBSKS,[27] which served as template. To construct shuttle vectors for baculovirus-mediated expression, we purified and ligated a 1075-bp EcoRI fragment spanning codon 29 to the C-terminus of the amplified mutated DNA with the 10-kb vector EcoRI fragment of pVL1392-His-tagged CCT-236. CCT-H301C-*2D* was generated by QuikChange using pVL1392-HisCT-H301C as template. Generation of the recombinant baculovirus used BaculoGold AcNPV DNA (PharMingen) and expression in *Trichoplusia ni* cells followed published procedures.[19]

CCT-T207C was also engineered using QuikChange mutagenesis and the cysteine-free template as above but was transferred to a pAX142 vector for expression in COS cells using MluI and SalI (which flank the coding region) to replace the WT CCT sequence. CCT-S288C-*8Ser* was engineered in two QuikChange mutagenesis steps using a cysteine-less construct in pAX-142. Primers introduced serine substitutions at codons 285, 286, 289, 290, 292, and 293 and a cysteine at codon 288 in the first round of amplification. Using this mutant DNA as template, another set of primers introduced serines at codons 275 and 278. This CCT variant and the CCT-T207C variant were expressed in COS cells for 48 h as previously described.[36] The full-length single-cysteine constructs contained His tags followed by a linker peptide containing a Factor Xa cleavage site. The N-terminal sequence of all uncleaved CCTs is MAKHHHHHHIEGRSA-CCT start codon.

Untagged CCT-cat (also referred to as CCT-236) was also expressed in *T. ni* cells via baculovirus and purified as previously described.[19] The CCT tail constructs (M+P) containing a single tryptophan at codon 278 or at codon 302 were engineered by QuikChange mutagenesis using templates in pET14b that were described in Ref. 28 and mutagenic primers. These were expressed in *Escherichia coli* as His_6 fusions with a thrombin site in the linker region. His tags were cleaved before use. A CCT-312 construct was also incorporated into pET14b and expressed in *E. coli* by 3 h IPTG induction at 37 °C.

All CCTs (with three exceptions described below) were purified from the 10,000*g* supernatant fraction of cell

lysates by nickel-agarose affinity chromatography as previously described.[29] The fractions containing CCT were pooled and dialyzed against buffer D [20 mM NaH_2PO_4 (pH 7.4), 150 mM NaCl, 2 mM dithiothreitol, and 0.25 mM Triton X-100] prior to storage at −80 °C in small aliquots. Three CCT constructs (His-CCT-312, His-CCT-T207C, and His-CCT-S288C-*8Ser*) were mostly in the 10,000*g* pellet and were purified after solubilization with 8 M urea by Ni-agarose chromatography. Proteins were refolded while immobilized on the Ni-agarose using a 8 M to 0 M urea gradient in 50 mM NaH_2PO_4 (pH 8.0), 0.5 M NaCl, 0.25 mM Triton X-100, and 1 mM dithiothreitol at a slow rate over the period of 1.5 h. After renaturation, proteins were eluted by addition of 350 mM imidazole, 50 mM NaH_2PO_4 (pH 8.0), 100 mM NaCl, 0.25 mM Triton X-100, and 1 mM dithiothreitol and dialyzed against buffer D.

The concentration of purified CCT stocks was determined by the Bradford method.[42] CCT activity was measured as described previously[43] in the presence or absence of egg PC/egg PG (1/1) sonicated vesicles, prepared in 10 mM Tris (pH 7.4), 150 mM NaCl, and 1 mM ethylenediaminetetraacetic acid. Phospholipids were from Avanti Polar Lipids.

Photo-cross-linking analysis

BBP labeling and photo-irradiation of BBP-labeled samples

Of 10 single-cysteine CCT variants, 3 were not analyzed due to their inability to be modified by BBP (CCT-S282C) or high insolubility and low yield after purification (CCT-S233C and CCT-D255C). Cross-linking analysis was successful for the remaining constructs, shown in Fig. 5. Twenty micrograms (0.5 nmol) of His-tagged single-cysteine CCT variant in buffer D [20 mM NaH_2PO_4 (pH 7.4), 150 mM NaCl, 2 mM dithiothreitol, and 0.25 mM Triton X-100] was bound to 100 µL of washed Ni-agarose beads by rotation on a wheel at 5 rpm for 20 min. After the sedimentation of the beads by centrifugation at 600 rpm for 30 s, the supernatant was removed, and the Ni-beads with bound CCT were resuspended in 100 µL of 240 µM BBP (Toronto Research Chemicals) in DMSO, to provide a BBP-to-CCT molar ratio of ~50. The sample was vortexed briefly and centrifuged to pellet the beads. Supernatant containing excess BBP was removed, and the beads were washed once with pure DMSO, four times with equilibration buffer [50 mM NaH_2PO_4 (pH 8.0), 500 mM NaCl, and 0.25 mM Triton X-100], and once with wash buffer [10 mM Tris, 150 mM NaCl, and 0.25 mM Triton X-100 (pH 7.4)]. All washes were 100 µL. BBP-labeled CCT variants were then recovered from Ni-beads with 4×100 µL washes with 350 mM imidazole, 10 mM Tris (pH 7.4), 150 mM NaCl, and 0.25 mM Triton X-100 (pH 7.4). All steps after adding BBP were at room temperature and in the dark.

Sample recovered from the Ni-beads was further diluted with 400 µL wash buffer. Diluted BBP-labeled CCT was UV irradiated on ice in the cold room (4 °C) for 1 h, using a UV GL25 Mineralight UV lamp set at 366 nm (Ultraviolet Products), at a distance of ~1 cm. Time trials revealed that 1 h irradiation was needed for maximal BBP incorporation. For photolysis in the presence of lipid vesicles, the sample from the Ni-beads was diluted with 400 µL of 6 mM dioleoyl phosphatidylglycerol (DOPG) sonicated vesicles in 10 mM Tris (pH 7.4) and 150 mM NaCl, for 5 min prior to irradiation. The lipid-to-CCT molar ratio was about 4000:1.

Preparation of samples for MS

Delipidation. Delipidation of the samples that were irradiated in the presence of excess lipid was accomplished by two different methods. For CCT-S288C delipidation, a solvent extraction procedure was followed.[22] Solvent-extracted samples were reconstituted in dilution buffer [10 mM Tris, 150 mM NaCl, 175 mM imidazole, and 0.25 mM Triton X-100 (pH 7.4)]. For CCT-I272C and CCT-H301C delipidation, Triton X-100 was added to UV irradiated samples to a final concentration of 1%. The Triton–PG mixed micelles were removed during purification of biotinylated peptides, described in the following section.

Trypsin digestion and purification of BBP-labeled peptides. We digested 800 µL BBP-labeled and photo-cross-linked samples with trypsin using a trypsin-to-CCT weight ratio of 1:5 for 1 h at 37 °C. The digestion was quenched with 2 mM PMSF. Half of each sample was reduced with 10 mM DTT for 15 min at 37 °C and alkylated with 500 mM iodoacetic acid for 30 min at room temperature in the dark. The other half was untreated. CCT samples were mixed for 1 h at room temperature with 5 µL monomeric avidin beads (Pierce) that had been prepared according to the manufacturer's recommendations. Beads were washed extensively with 4×50 µL wash buffer [100 mM NaH_2PO_4 (pH 7), 150 mM NaCl, and 0.25 mM Triton X-100] and 2×100 µL ddH_2O. BBP-labeled peptides were then recovered with 4×5 µL acidic elution buffer [70% acetonitrile and 30% trifluoroacetic acid (TFA)].

MS and analysis

Purified BBP-labeled peptides were mixed 1:1 with 10 mg/mL α-cyano-4-hydroxycinnamic acid in acidic elution buffer and co-crystallized on sample wells of a MALDI target plate (Waters Instruments). In parallel, a standard mix containing angiotensin II (1047 Da), P14R (1534 Da), ACTH fragment 18–39 (2466 Da), insulin B chain (3496 Da), and insulin (5734 Da) was also mixed 1:1 (v/v) with 10 mg/mL α-cyano-4-hydroxycinnamic acid in elution buffer and co-crystallized on a MALDI target plate. Samples were dried at room temperature in the dark. Mass spectra were collected on a MALDI-TOF-mass spectrometer (MALDI-LR; Waters Technologies) equipped with delayed ion extraction and operated in linear mode. For all samples, the source voltage was 15 kV, the detector voltage was 1.8 kV, and the delay time was 500 ns. The mass range was set at 700–10,000 Da. Each mass spectrum was the sum of at least 200 laser shots. MS-Digest program was used to calculate the theoretical mass of tryptic digests of different CCT constructs†. The program MassLynx‡ was used to visualize MS data. All peak matching and identification were done manually. The parameters used to evaluate peptide masses included the following potential modifications: oxidation of methionine, acetylation of N-terminus of protein, phosphorylation, acetamide alkylation, and reduction without subsequent alkylation. The methods for determining the converging

point of BBP-mediated cross-links on the catalytic domain are described in detail in the legend to Fig. S3 in Supplementary Material.

H/D exchange MS and comparative analysis of CCT-cat and CCT-312

CCT-cat spans residues 1–236 (no M domain), and CCT-312 spans residues 1–312, including the M domain. These truncated CCTs had WT sequence. Quadruplicate aliquots (1.2 μL or ~350 pmol) of CCT-cat or CCT-312 in 10 mM Tris (pH 7.4), 150 mM NaCl, 1 mM ethylenediaminetetraacetic acid, and 2 mM DTT were mixed with 4.8 μL of 10 mM Tris (pH 8.0) and 2 μL D_2O, and the samples were placed immediately in a water bath at 20 °C for 2 min. Samples were quenched with 10 μL of 250 mM tris(2-carboxyethyl)phosphine–HCl in 0.08% TFA (pH 2.3) and immediately injected into a 10-μL loop connected to an immobilized pepsin reactor (Applied Biosystems, Concord, ON, Canada). Samples were pumped through the digestion column using 3% acetonitrile, 0.03% trifluoroacetate, and 0.02% formic acid, at 4 μL/min. Upon exiting the column, the cleaved peptides entered a C18 reversed-phase column and were separated using a step gradient of 5–90% acetonitrile in 0.03% TFA and 0.02% formic acid over 14 min. All chromatography was done at 0–4 °C. The separated peptides were directly infused into a QSTAR Pulsar *i* quadrupole TOF mass spectrometer. Spectra of non-deuterated CCT peptides were identified under these same conditions by tandem MS/MS and database searching. Data were collected using Analyst QS™ version 1.1 (Applied Biosystems). We used MASCOT 2.1§ to search the CCT sequence for *in silico* digest matches to the experimentally acquired peptide masses. Our identification criteria were ± 0.5 amu mass tolerance in MS and 0.8 amu mass tolerance in MS/MS. The MASCOT search identified 57 peptides in CCT(1–236) and 68 peptides in CCT(1–312), which were modified to varying degrees by incremental mass units. Mass spectral data from each replicate H/D exchange MS run were analyzed using Hydra software,[44,45] using the method described by Ling *et al.*[45] Mass shift significance was evaluated using methods described in Bennett *et al.*[46]

Fluorescence analyses

Labeling with OG

His-tagged single-cysteine variants (1.2–5 nmol) in dialysis buffer [20 mM NaH_2PO_4 (pH 7.4), 150 mM NaCl, 1 mM DTT, and 0.25 mM Triton X-100] were bound to 100 μL of prepared Ni-beads for 20 min at room temperature. After centrifugation at 600 rpm for 30 s, the supernatant was removed and the Ni-beads with bound CCT were resuspended in 100 μL equilibration buffer [50 mM NaH_2PO_4 (pH 8.0), 500 mM NaCl, and 0.25 mM Triton X-100] containing 0.05–0.24 nmol OG 488-IAA (Invitrogen). After vortexing and sedimentation as above, the supernatant containing excess OG was removed. Beads were washed 10 times with equilibration buffer and once with wash buffer [10 mM Tris (pH 7.4), 150 mM NaCl, and 0.25 mM Triton X-100]. All washes were of 100 μL volume. OG-labeled CCT was recovered from the Ni-beads with 4×100 μL elution buffer [350 mM imidazole, 10 mM Tris (pH 7.4), 150 mM NaCl, and 0.25 mM Triton X-100]. Recovered sample was further diluted with 400 μL wash buffer and aliquoted for different analyses.

Determination of OG percent labeling

The OG concentration was obtained from an absorbance scan from 400 to 550 nm. A background scan was performed on sample buffer [10 mM Tris (pH 7.4), 150 mM NaCl, 0.25 mM Triton X-100, and 175 mM imidazole]. Background-corrected peak absorbance at around 491 nm was used to calculate OG concentration using a molar extinction coefficient of 70,000 M^{-1} cm^{-1}. Protein concentration was determined by Bradford.[42] The percent of CCT labeled by OG was calculated as: 100%×(OG concentration)/(protein concentration).

Steady-state anisotropy measurements

Fluorescence data were acquired using a Horiba Jobin Yvon FluoroLog 3 spectrometer equipped with polarizers. The limiting anisotropy (r_o) value for OG was determined by analysis in glycerol at −10 °C. The value obtained was 0.381±0.002. This is in agreement with published values for fluorescein or OG.[47] The OG-labeled CCT sample (110 μL) in a quartz cuvette was equilibrated to 20 °C in the thermally controlled sample chamber for 5 min. We also measured the anisotropy of unlabeled CCTs using intrinsic tryptophan fluorescence: CCT-cat (monitoring W-151) and CCT tails (monitoring W-278 or W-302). The instrument settings for OG fluorescence were as follows: excitation wavelength, 491 nm; emission wavelength, 522 nm; excitation and emission slit widths, 8 nm; integration time, 1 s. The settings for tryptophan fluorescence were as follows: excitation wavelength, 295 nm; emission wavelength, 348 nm; excitation and emission slit widths, 12 nm; integration time, 1 s. Six anisotropy readings were recorded for each sample.

Urea denaturation analysis

The anisotropy of the CCT sample (110 μL) was acquired in the absence of urea, as above. The sample was then transferred sequentially to 10 tubes each containing 5 mg dried ultrapure urea to a final urea concentration of 8.3 mM. After each transfer, the sample was vortexed and equilibrated at 20 °C with the urea for 5 min. A test trial showed that this time was sufficient to reach a folding/unfolding equilibrium. Anisotropy was measured as described above for undenatured samples.

Other methods

Preparation of CCT-cat/CCT-S288C heterodimer

This heterodimer was prepared as previously described[29] with modifications. We mixed SDS-denatured, Strep-tagged CCT-cat (truncated before M domain) with His-tagged CCTS288C (full length). Purification utilized Ni-agarose to remove the His-tagged full-length homodimers. The

unbound fraction contained a mixture of Strep-tagged CCT-cat homodimers and Strep-tagged CCT-cat/His CCT-S288C heterodimers, and this fraction was used for copper phenanthroline-mediated disulfide formation. Since our detection method utilized an anti-domain M antibody and was thus selective for the heterodimer, it was not necessary to separate heterodimer from CCT-cat homodimer.

Oxidation with copper phenanthroline

We prepared 5 mM $CuSO_4$ and 15 mM 1,10-phenanthroline stocks in ddH_2O and mixed them to form $Cu(Phe)_3$ immediately prior to use following Xie *et al.*[27] Samples containing 0.8 μM CCT in 30 μL of 20 mM NaH_2PO_4 (pH 7.4), 150 mM NaCl, and 0.25 mM Triton X-100 were reacted with 0.2 mM $Cu(Phe)_3$ for 10 min at 37 °C with shaking. The reaction was quenched with freshly prepared alkylating reagent, IAA (20 mM). For pre-quenched samples, the IAA treatment preceded the addition of the $Cu(Phe)_3$. Samples were analyzed by 10% SDS-PAGE.

Acknowledgements

We are grateful to Ziwei Ding for assistance with the design and preparation of CCT full-length constructs, Joseph Lee for preparation of the CCT tail constructs, and George Agnes for technical training, advice, and use of the MALDI-MS instrumentation. This work is supported by a grant from the Canadian Institutes of Health Research to R.B.C. and a Canadian Institutes of Health Research resource grant to D.C.S.

Supplementary Data

Supplementary data to this article can be found online at http://dx.doi.org/10.1016/j.jmb.2012.12.003

Received 4 October 2012;
Received in revised form 24 November 2012;
Accepted 3 December 2012
Available online 10 December 2012

Keywords:
auto-inhibition;
cytidylyltransferase;
photo-cross-linking;
fluorescence anisotropy;
mass spectrometry

Present addresses: H. K-H. Huang, Department of Animal Biology, School of Veterinary Medicine, University of Pennsylvania, 3850 Baltimore Avenue, Philadelphia, PA 19104–6009, USA;
L. P. Silva, Department of Bioinformatics and Computational Biology, MD Anderson Cancer Center, University of Texas, Houston, TX 77054, USA.

† http://prospector.ucsf.edu/prospector/cgi-bin/msform.cgi?form=msdigest
‡ www.micromass.co.uk
§ http://www.matrixscience.com

Abbreviations used:
CCT, CTP:phosphocholine cytidylyltransferase; BBP, 2-[*N*-α-benzoylbenzoicamido-N^6-(6-biotinamidocaproyl)-L-lysinylamido]ethyl methane thiosulfonate; AI, auto-inhibitory; DMSO, dimethyl sulfoxide; IAA, iodoacetamide; HRP, horseradish peroxidase; PC, phosphatidylcholine; MALDI, matrix-assisted laser desorption/ionization; MS, mass spectrometry; PDB, Protein Data Bank; H/D, hydrogen/deuterium; TOF, time of flight; DOPG, dioleoyl phosphatidylglycerol; PG, phosphatidylglycerol; OG, Oregon Green; WT, wild type; TFA, trifluoroacetic acid.

References

1. Smock, R. G. & Gierasch, L. M. (2009). Sending signals dynamically. *Science*, **324**, 198–203.
2. Dyson, H. J. & Wright, P. E. (2002). Coupling of folding and binding for unstructured proteins. *Curr. Opin. Struct. Biol.* **12**, 54–60.
3. Cheng, C. Y., Yang, J., Taylor, S. S. & Blumenthal, D. K. (2009). Sensing domain dynamics in protein kinase A-Iα complexes by solution X-ray scattering. *J. Biol. Chem.* **284**, 35916–35925.
4. Tompa, P. & Fuxreiter, M. (2008). Fuzzy complexes: polymorphism and structural disorder in protein–protein interactions. *Trends Biochem. Sci.* **33**, 2–8.
5. Baker, J. M., Hudson, R. P., Kanelis, V., Choy, W. Y., Thibodeau, P. H., Thomas, P. J. & Forman-Kay, J. D. (2007). CFTR regulatory region interacts with NBD1 predominantly via multiple transient helices. *Nat. Struct. Mol. Biol.* **14**, 738–745.
6. Mittag, T., Orlicky, S., Choy, W. Y., Tang, X., Lin, H., Sicheri, F. *et al.* (2008). Dynamic equilibrium engagement of a polyvalent ligand with a single-site receptor. *Proc. Natl Acad. Sci. USA*, **105**, 17772–17777.
7. Johnson, J. E. & Cornell, R. B. (1999). Amphitropic proteins: regulation by reversible membrane interactions (review). *Mol. Membr. Biol.* **16**, 217–235.
8. Cornell, R. B. & Northwood, I. C. (2000). Regulation of CTP:phosphocholine cytidylyltransferase by amphitropism and relocalization. *Trends Biochem. Sci.* **25**, 441–447.
9. Jamil, H., Hatch, G. M. & Vance, D. E. (1993). Evidence that binding of CTP:phosphocholine cytidylyltransferase to membranes in rat hepatocytes is modulated by the ratio of bilayer- to non-bilayer-forming lipids. *Biochem. J.* **291**, 419–427.
10. Jamil, H., Yao, Z. M. & Vance, D. E. (1990). Feedback regulation of CTP:phosphocholine cytidylyltransferase translocation between cytosol and endoplasmic reticulum by phosphatidylcholine. *J. Biol. Chem.* **265**, 4332–4339.
11. Cornell, R. B. (1998). How cytidylyltransferase uses an amphipathic helix to sense membrane phospholipid composition. *Biochem. Soc. Trans.* **26**, 539–544.

12. Cornell, R. B. & Taneva, S. G. (2006). Amphipathic helices as mediators of the membrane interaction of amphitropic proteins, and as modulators of bilayer physical properties. *Curr. Protein Pept. Sci.* **7**, 539–552.
13. Leonard, T. A. & Hurley, J. H. (2011). Regulation of protein kinases by lipids. *Curr. Opin. Struct. Biol.* **21**, 785–791.
14. Neumann, P., Weidner, A., Pech, A., Stubbs, M. T. & Tittmann, K. (2008). Structural basis for membrane binding and catalytic activation of the peripheral membrane enzyme pyruvate oxidase from *Escherichia coli*. *Proc. Natl Acad. Sci. USA*, **105**, 17390–17395.
15. Wang, Y. & Kent, C. (1995). Identification of an inhibitory domain of CTP:phosphocholine cytidylyltransferase. *J. Biol. Chem.* **270**, 18948–18952.
16. Friesen, J. A., Campbell, H. A. & Kent, C. (1999). Enzymatic and cellular characterization of a catalytic fragment of CTP:phosphocholine cytidylyltransferase α. *J. Biol. Chem.* **274**, 13384–13389.
17. Ding, Z., Taneva, S. G., Huang, H. K.-H., Campbell, S., Semenec, L., Chen, N. & Cornell, R. B. (2012). A 22mer segment in the structurally pliable regulatory domain of metazoan CTP: phosphocholine cytidylyltransferase facilitates both silencing and activating functions. *J. Biol. Chem.* **287**, 38980–38991.
18. Dunne, S. J., Cornell, R. B., Johnson, J. E., Glover, N. R. & Tracey, A. S. (1996). Structure of the membrane binding domain of CTP:phosphocholine cytidylyltransferase. *Biochemistry*, **35**, 11975–11984.
19. Taneva, S., Johnson, J. E. & Cornell, R. B. (2003). Lipid-induced conformational switch in the membrane binding domain of CTP:phosphocholine cytidylyltransferase: a circular dichroism study. *Biochemistry*, **42**, 11768–11776.
20. Yang, W., Boggs, K. P. & Jackowski, S. (1995). The association of lipid activators with the amphipathic helical domain of CTP:phosphocholine cytidylyltransferase accelerates catalysis by increasing the affinity of the enzyme for CTP. *J. Biol. Chem.* **270**, 23951–23957.
21. Lee, J., Johnson, J., Ding, Z., Paetzel, M. & Cornell, R. B. (2009). Crystal structure of a mammalian CTP: phosphocholine cytidylyltransferase catalytic domain reveals novel active site residues within a highly conserved nucleotidyltransferase fold. *J. Biol. Chem.* **284**, 33535–33548.
22. Bogan, M. J., Agnes, G. R., Pio, F. & Cornell, R. B. (2005). Interdomain and membrane interactions of CTP:phosphocholine cytidylyltransferase revealed via limited proteolysis and mass spectrometry. *J. Biol. Chem.* **280**, 19613–19624.
23. Dennis, M. K., Taneva, S. G. & Cornell, R. B. (2011). The intrinsically disordered nuclear localization signal and phosphorylation segments distinguish the membrane affinity of two cytidylyltransferase isoforms. *J. Biol. Chem.* **286**, 12349–12360.
24. Braker, J. D., Hodel, K. J., Mullins, D. R. & Friesen, J. A. (2009). Identification of hydrophobic amino acids required for lipid activation of *C. elegans* CTP: phosphocholine cytidylyltransferase. *Arch. Biochem. Biophys.* **492**, 10–16.
25. Ahrends, R., Kosinski, J., Kirsch, D., Manelyte, L., Giron-Monzon, L., Hummerich, L. *et al.* (2006). Identifying an interaction site between MutH and the C-terminal domain of MutL by crosslinking, affinity purification, chemical coding and mass spectrometry. *Nucleic Acids Res.* **34**, 3169–3180.
26. Guo, L. W., Muradov, H., Hajipour, A. R., Sievert, M. K., Artemyev, N. O. & Ruoho, A. E. (2006). The inhibitory γ subunit of the rod cGMP phosphodiesterase binds the catalytic subunits in an extended linear structure. *J. Biol. Chem.* **281**, 15412–15422.
27. Xie, M., Smith, J. L., Ding, Z., Zhang, D. & Cornell, R. B. (2004). Membrane binding modulates the quaternary structure of CTP:phosphocholine cytidylyltransferase. *J. Biol. Chem.* **279**, 28817–28825.
28. Taneva, S. G., Lee, J. M. & Cornell, R. B. (2012). The amphipathic helix of an enzyme that regulates phosphatidylcholine synthesis remodels membranes into highly curved nanotubules. *Biochim. Biophys. Acta*, **1818**, 1173–1186.
29. Taneva, S., Dennis, M. K., Ding, Z., Smith, J. L. & Cornell, R. B. (2008). Contribution of each membrane binding domain of the CTP:phosphocholine cytidylyltransferase-α dimer to its activation, membrane binding, and membrane cross-bridging. *J. Biol. Chem.* **283**, 28137–28148.
30. Pattridge, K. A., Weber, C. H., Friesen, J. A., Sanker, S., Kent, C. & Ludwig, M. L. (2003). Glycerol-3-phosphate cytidylyltransferase. Structural changes induced by binding of CDP-glycerol and the role of lysine residues in catalysis. *J. Biol. Chem.* **278**, 51863–51871.
31. Helmink, B. A., Braker, J. D., Kent, C. & Friesen, J. A. (2003). Identification of lysine 122 and arginine 196 as important functional residues of rat CTP:phosphocholine cytidylyltransferase α. *Biochemistry*, **42**, 5043–5051.
32. Lakowicz, J. R. (2006). Principles of Fluorescence Spectroscopy, 3rd edit. Springer, New York, NY.
33. Weber, C. H., Park, Y. S., Sanker, S., Kent, C. & Ludwig, M. L. (1999). A prototypical cytidylyltransferase: CTP:glycerol-3-phosphate cytidylyltransferase from *Bacillus subtilis*. *Structure*, **7**, 1113–1124.
34. Fuxreiter, M., Simon, I., Friedrich, P. & Tompa, P. (2004). Preformed structural elements feature in partner recognition by intrinsically unstructured proteins. *J. Mol. Biol.* **338**, 1015–1026.
35. Friesen, J. A., Liu, M. F. & Kent, C. (2001). Cloning and characterization of a lipid-activated CTP:phosphocholine cytidylyltransferase from *Caenorhabditis elegans*: identification of a 21-residue segment critical for lipid activation. *Biochim. Biophys. Acta*, **1533**, 86–98.
36. Johnson, J. E., Xie, M., Singh, L. M., Edge, R. & Cornell, R. B. (2003). Both acidic and basic amino acids in an amphitropic enzyme, CTP:phosphocholine cytidylyltransferase, dictate its selectivity for anionic membranes. *J. Biol. Chem.* **278**, 514–522.
37. Gehrig, K., Cornell, R. B. & Ridgway, N. D. (2008). Expansion of the nucleoplasmic reticulum requires the coordinated activity of lamins and CTP:phosphocholine cytidylyltransferase α. *Mol. Biol. Cell*, **19**, 237–247.
38. Gautier, R., Douguet, D., Antonny, B. & Drin, G. (2008). HELIQUEST: a web server to screen sequences with specific α-helical properties. *Bioinformatics*, **24**, 2101–2102.

39. Antz, C., Geyer, M., Fakler, B., Schott, M. K., Guy, H. R., Frank, R. *et al.* (1997). NMR structure of inactivation gates from mammalian voltage-dependent potassium channels. *Nature*, **385**, 272–275.
40. Hoshi, T., Zagotta, W. N. & Aldrich, R. W. (1990). Biophysical and molecular mechanisms of Shaker potassium channel inactivation. *Science*, **250**, 533–538.
41. Zagotta, W. N., Hoshi, T. & Aldrich, R. W. (1990). Restoration of inactivation in mutants of Shaker potassium channels by a peptide derived from ShB. *Science*, **250**, 568–571.
42. Bradford, M. M. (1976). A rapid and sensitive method for the quantitation of microgram quantities of protein utilizing the principle of protein-dye binding. *Anal. Biochem.* **72**, 248–254.
43. Sohal, P. S. & Cornell, R. B. (1990). Sphingosine inhibits the activity of rat liver CTP: phosphocholine cytidylyltransferase. *J. Biol. Chem.* **265**, 11746–11750.
44. Slysz, G., Baker, C., Bozsa, B., Dang, A., Percy, A., Bennett, M. & Schriemer, D. (2009). Hydra: software for tailored processing of H/D exchange data from MS or tandem MS analyses. *BMC Bioinformatics*, **10**, 162–176.
45. Ling, J., Shima, C., Schriemer, D. & Schryvers, A. (2010). Delineating the regions of human transferrin involved in interactions with transferrin binding protein B from *Neisseria meningitidis*. *Mol. Microbiol.* **77**, 1301–1314.
46. Bennett, M., Barakat, K., Huzil, J., Tuszynski, J. & Schriemer, D. (2010). Discovery and characterization of the laulimalide-microtubule binding mode by mass shift perturbation mapping. *Chem. Biol.* **17**, 725–734.
47. Rusinova, E., Tretyachenko-Ladokhina, V., Vele, O. E., Senear, D. F. & Alexander Ross, J. B. (2002). Alexa and Oregon Green dyes as fluorescence anisotropy probes for measuring protein–protein and protein–nucleic acid interactions. *Anal. Biochem.* **308**, 18–25.